

RECOVERY OF SURFACE STRUCTURES FROM NEAR-FIELD OPTICAL INTENSITIES

N. GARCIA (1) AND M. NIETO-VESPERINAS (2)

(1) *Física de Sistemas Pequeños, C.S.LC.,*

(2) *Instituto de Ciencia de Materiales, Sede B,
C.S.LC. and Departamento de Física de la Materia
Condensada, Facultad de Ciencias C-III, Universidad
Autónoma, Cantoblanco, Madrid 28049, Spain.*

ABSTRACT. We demonstrate the difficulty associated to the reconstruction of surface topography of objects under multiple scattering conditions. Specifically, the image of the near field detected by a tip does not follow the object profile. We put forward two different methods to reconstruct the object. One is an inverse scattering technique, based on the Rayleigh hypothesis, which requires to find the phase of the scattered field, and the other, which does not use neither phase retrieval nor inverse scattering, is done by integration of near-field optical intensities over all possible angles of incidence of the illuminating wave.

1. Introduction

The reconstruction of an object from wave scattering data is a well known problem of relevance in many areas of science. Detectors only retrieve intensities, and therefore in experimental measurements the phase of the scattered field is lost. When single scattering takes place, holography was originally proposed by Gabor to overcome this problem [1], and has quite successfully been developed ever since [2] - [5]. In addition, numerical procedures, have been put forward both for light and x-rays [6] - [7] as alternatives to holography when there is no reference wave available. It is, however, well known that when multiple scattering occurs, even if the phase of the scattered field is known, the inversion procedure is quite involved and, to date, only approximate solutions have been put forward for some particular cases [8]-[10]. Recently, the difficulties involved in potential recovery from low energy electron diffraction have been discussed [11]-[12]. We address here the reconstruction of the surface profile that separates two half spaces with different refractive index. It is shown that the near field intensity of the scattered field, does not follow the subject profile. The reconstruction of the object is, however, possible. We put forward two different procedures. The first one is an inverse scattering method, of use when the phase of the scattered field is known; the second one is a procedure that does not require neither phase retrieval nor inverse scattering techniques, and that shows that the near field intensity, integrated over all possible angles of incidence of the impinging wave, closely follows the profile of this surface, even under multiple scattering conditions. This overcomes both the problem of phase retrieval and of inverse scattering from complex amplitude data.

2. The Inverse Scattering Procedure

Given a collection of multiply scattered intensity data, the reconstruction of the profile of an interface, separating two media of different refractive index, has been so far tackled only for perfectly conducting surfaces by means of an iterative logarithmic transformation [13]. However, this procedure requires knowledge of the phase of the scattered field. Only for retrieval of statistical parameters of a

random surface, (e.g. standard deviation and correlation length of the random heights) there is an inversion procedure based on just knowledge of the intensity [14]. It should be recalled that this question is of general interest and appears in such diverse fields as light scattering, remote sensing, oceanography, electromagnetics, integrated optics, acoustics, solid state physics and particle detection [15]-[21].

Here we establish a procedure for retrieving the local structure of the interface that separates two media of different refractive index from only data of the scattered intensities; with multiple scattering and even if both media are penetrable.

Let the object consist of a corrugated surface with profile given by the height variation $z = D(\mathbf{R})$, $\mathbf{R} = (x, y)$. In the illustration shown in this work, we shall consider a one-dimensional boundary surface separating two media of different dielectric permittivity ε , (see Fig.1). We shall carry out the calculations for a periodic profile D illuminated by a plane wave incident on a plane perpendicular to the grooves: $U^{(i)}(\mathbf{r}) = \exp[i(\mathbf{K}_i \cdot \mathbf{R} + k_{iz}z)]$; ($|\mathbf{k}_i|^2 = K_i^2 + k_{iz}^2 = k^2$, $k^2 = k_0^2 \sqrt{\varepsilon}$, $k_0^2 = (2\pi/\lambda)^2$). Note that for an electromagnetic wave, the scalar representation used here is valid for either TE or TM polarization. Thus the scattered field can be described by the complex amplitude $U(\mathbf{r}, \mathbf{K}_i)$, ($\mathbf{r} = (x, y, z)$). At points outside the selvedge this function admits the representation in terms of an angular spectrum $A(\mathbf{K}, \mathbf{K}_i)$ of plane waves outgoing from the surface [5]:

$$U(\mathbf{R}, z; \mathbf{K}_i) = \int_{-\infty}^{\infty} A(\mathbf{K}, \mathbf{K}_i) \exp[i(\mathbf{K} \cdot \mathbf{R} + k_z z)] d\mathbf{K}, \quad (1)$$

where $k_z = \sqrt{k^2 - K^2}$, for $K^2 < k^2$ (propagating components), and $k_z \equiv \kappa_E = i\sqrt{K^2 - k^2}$, for $K^2 > k^2$ (evanescent components). Any scattered field has necessarily both kinds of waves [26]. For the case of a periodic surface, $A(\mathbf{K}, \mathbf{K}_i)$ has discrete values at $\mathbf{K} \equiv \mathbf{K}_G = \mathbf{K}_i + \mathbf{G}$, with $G = (2\pi/a)n$, (a and n being the profile period and an integer, respectively). Namely, the diffracted amplitudes are:

$$A(\mathbf{K}, \mathbf{K}_i) \equiv A_G = (1/k_{Gz}) \int_{-a/2}^{a/2} F(\mathbf{R}; \mathbf{K}_i) \exp[-i(\mathbf{K}_G \cdot \mathbf{R} + k_{Gz}z)] d\mathbf{R}. \quad (2)$$

In Eq.(2) $K_G^2 + k_{Gz}^2 = k^2$ and $F(\mathbf{R}; \mathbf{K}_i)$ is the induced source function.

As seen from Eq.(1), due to the factor $\exp(-k_z z)$ appearing in the integrand for $K^2 > k^2$, the evanescent components are lost for $z \gg \lambda$.

The Rayleigh hypothesis on which we base our inverse scattering method, [27] states the validity of Eq.(1) within the selvedge, and in particular, at points in the surface. Hence, the extinction theorem boundary condition [28], reads:

$$\exp(ik_{iz}D(\mathbf{R})) + \sum_{\mathbf{G}} A_G \exp[i(\mathbf{G} \cdot \mathbf{R} + k_{Gz}D(\mathbf{R}))] = 0. \quad (3)$$

Eq.(3) suggests the following iterative scheme for retrieval of $D(\mathbf{R})$ from the amplitudes A_G :

$$D_n(\mathbf{R}) = (1/2k_{iz}) \ln \left| - \sum_{\mathbf{G}} A_G \exp(i\mathbf{G} \cdot \mathbf{R}) \exp[i(k_{Gz} - k_{iz}D_{n-1}(\mathbf{R}))] \right|. \quad (4)$$

The 0th iteration being:

$$D_0(\mathbf{R}) = (1/2k_{iz}) \ln \left| - \sum_{\mathbf{G}} A_G \exp(i\mathbf{G} \cdot \mathbf{R}) \right| \quad (5)$$

Eqs. (4)- (5) were proposed in Ref. 29 for inversion from knowledge of the far field amplitudes A_G ; (namely, for k_{Gz} real). Here we show its use from knowledge of both the far field (homogeneous or propagating) amplitudes and the evanescent (non-propagating) A_G 's. We shall show that it is precisely the inclusion of these evanescent wave components in the detection what permits reconstructions with superresolution. Both kinds of angular components given by the complex amplitudes $A(\mathbf{K}) \exp(ik_z z_0)$ are retrieved from the NFO detected field $U(\mathbf{R}, z_0)$ by a 2-D inverse Fourier transform of Eq. (1) .

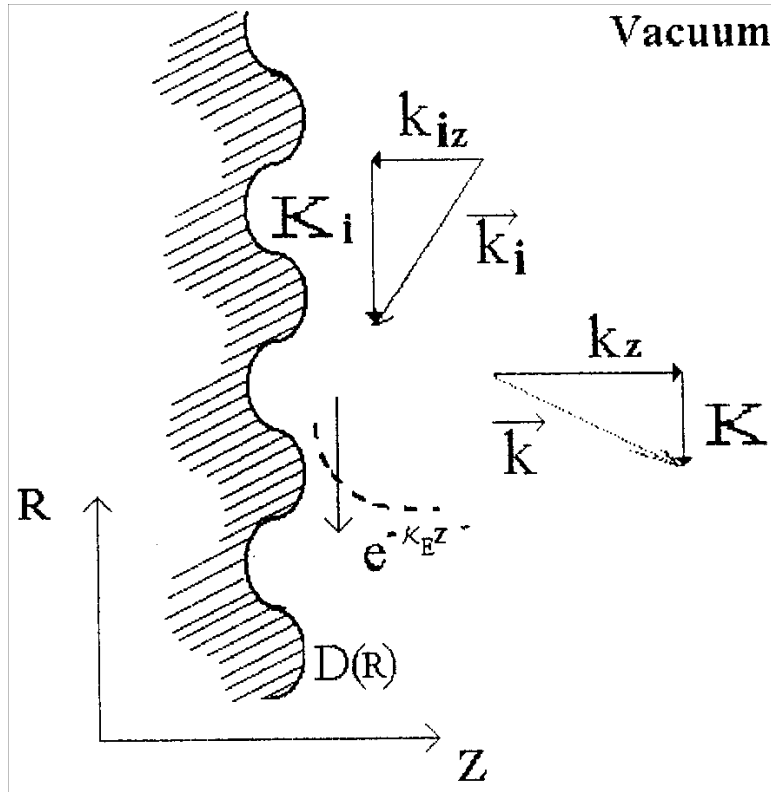
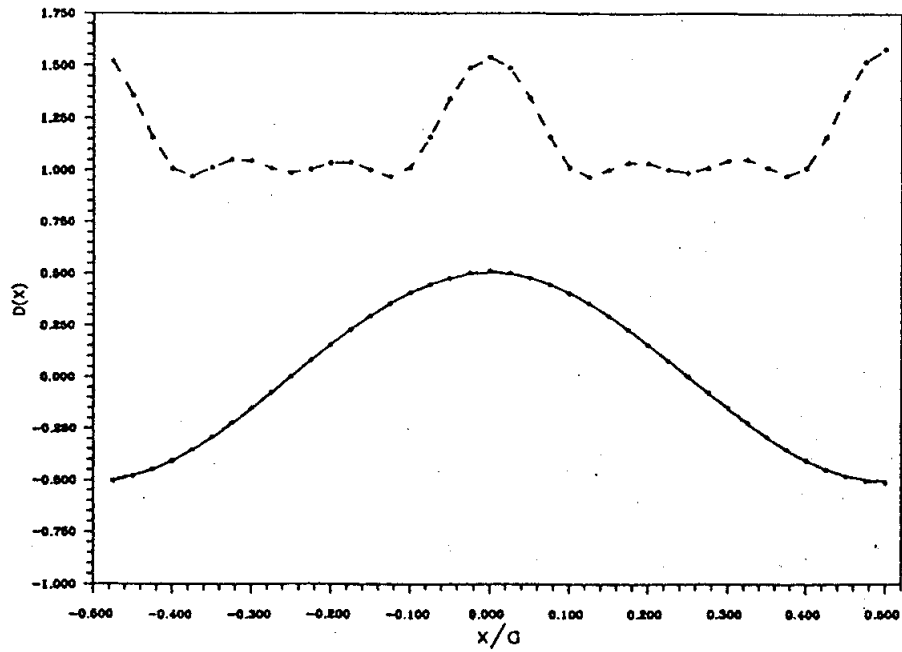
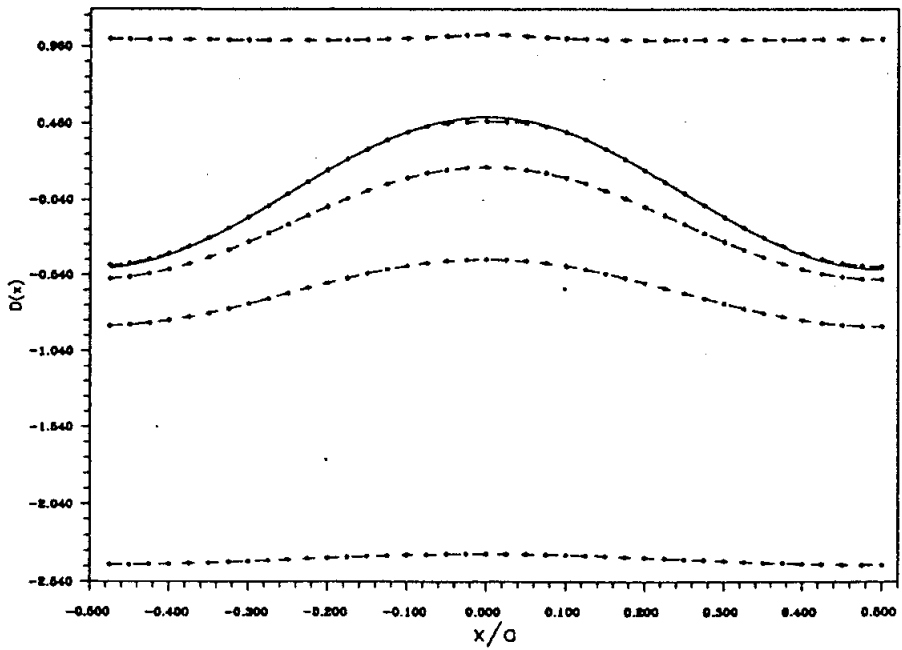


Figure 1. Scattering Geometry

We next show numerical simulations illustrating the above remarks. A test profile $D(x)$ is introduced. The angular spectrum A_G is evaluated from the Rayleigh equation (3). The field $U(\mathbf{R}, z_0)$ is then simulated by means of Eq. (1). We first present results for $D(x) = h \cos(2\pi x/a)$. Fig. 2 (a) corresponds to $a = 3.18\lambda$ and $h = 0.25\lambda$ and shows: (i) one period of this profile, (ii) the modulus of the field $U(\mathbf{R}, z_0)$ at $z_0 = h$, which is the measured quantity, and (iii) the reconstruction of $D(x)$ from this field by first getting the A_G 's by inverse Fourier transforming Eq.(1) and then using the iterative Eqs.(4) and (5). As seen, the field U at $z_0 = h$ does not resemble at all the surface profile. Observe that it is precisely this squared modulus, i.e. the field intensity, what would be seen if one made an optical image of the surface. On the other hand, the reconstruction of $D(x)$ is quite good, even though the ratio $h/a = 0.08$ slightly surpasses the Rayleigh criterion in this case. We have performed calculations with values of z_0 up to infinity, with very similar results. In this case, a is large enough so that no evanescent components are necessary to recover the profile. However, for smaller a , the value of z_0 becomes critical for a successful subwavelength reconstruction. Fig. 2 (b) shows the reconstructions of the same profile, this time with $a = 0.16\lambda$ and $h = 0.012\lambda$, for several values of the detection distance: $z_0 = 0, h, 3h$ and $10h$, at all of which the scattered field modulus remains almost constant at z_0 . As seen, the resolution of the reconstructed $D(x)$ is gradually lost as z_0 increases from the ideal situation $z_0 = 0$, (all evanescent components included), up to $z = 10h$.



(a)



(b)

Figure 2. (a) The solid curve is test profile $D(x) = h[\cos(2\pi x/a)]$ for $a = 3.18\lambda$, $h/a = 0.08$. The dashed curve coincident on the test profile is the reconstructed profile from the scattered field at $z_0 = h$ and the upper dashed curve is the scattered field at $z_0 = h$. (b) Same as (a) for $a = 0.16\lambda$, $h/a = 0.08$. Lower dashed curves from top to bottom are the reconstructed profiles from $z_0 = 0, h, 3h$, and $10h$, respectively. The upper dashed curve is the scattered field at $z_0 = h$.

3. Integration of the Near Field Intensity over the Angles of Incidence

This second method is based on a result which shows that the scattered intensity, integrated over all possible angles of incidence of the impinging incident wave, tends to a constant at distances many wavelengths far from the object, and follows the local surface topography at short distances from it, of the order of a few wavelengths. In this connection, it should be remarked that for instance near field optics is a technique which is receiving intense study [22]-[25] as a procedure to overcome the Rayleigh limit of resolution of conventional optics; however, at present it still has some difficulties due to the unavoidable presence of multiple scattering in subwavelength structures [13]. Therefore, *near field detection, incorporating the integration operation presented in this letter, constitutes a means to automatically retrieve the surface profile without phase retrieval nor inverse scattering calculations, even if there is multiple scattering or diffraction.*

For arguments \mathbf{K} and \mathbf{K}' in the domain of propagating components, namely, for $K^2 < k^2$, and $K'^2 < k^2$, and $z \gg \lambda$, the method of the stationary phase makes the measured scattered intensity outside the selvedge $I(\mathbf{R}, z; \mathbf{K}_i) = k_{iz} / k |U(\mathbf{R}, z; \mathbf{K}_i)|^2$, integrated over all angles of incidence given by the incident \mathbf{K} -vector \mathbf{K}_i , to give rise to the function $I_T(\mathbf{R}, z)$:

$$I_T(\mathbf{R}, z) \cong \int \int_{\text{homog}} \frac{k_{iz}}{k} \exp[i(\mathbf{K} - \mathbf{K}') \cdot \mathbf{R}] |A(\mathbf{K})|^2 \delta(\mathbf{K} - \mathbf{K}') d\mathbf{K} d\mathbf{K}'. \quad (6)$$

Whereas for arguments \mathbf{K} and \mathbf{K}' in the domain of both propagating and evanescent components, and $z \sim \lambda$, one has:

$$I_T(\mathbf{R}, z) = \int_{-\infty}^{\infty} \int_{-\infty}^{\infty} \exp[i(\mathbf{K} - \mathbf{K}') \cdot \mathbf{R}] g(\mathbf{K}, \mathbf{K}', z) d\mathbf{K} d\mathbf{K}'. \quad (7)$$

$g(\mathbf{K}, \mathbf{K}', z)$ being a function that depends on the distance z to the sample. In Eq. (6) *homog* indicates that the integration is done in the propagating component domain, only.

Hence, the integrated intensity is approximately constant at those values of z far enough from the source, so that evanescent components are lost; and it is a function of z at those values of z close enough to the surface so that both evanescent components and those components near the cut-off: $K^2 = k^2$ are retrieved. In addition, $I_T(\mathbf{R}, z)$ very closely follows the surface profile for $z \cong \lambda$ as we shall next show in the following numerical simulations.

We introduce a test profile $D(x)$. For an incident plane wave $U^{(i)}(\mathbf{r}) = \exp[i(\mathbf{K}_i \cdot \mathbf{R} + k_{iz}z)]$ the angular spectrum A_G is evaluated by means of the Rayleigh method [27] which is exact in the range of parameters used here, [13]. The scattered field $U(\mathbf{R}, z_0; \mathbf{K}_i)$ is then simulated at several distances z_0 by means of Eq.(1), and then the intensity $I_T(\mathbf{R}, z)$ is obtained by integrating the scattered intensity $I(\mathbf{R}, z; \mathbf{K}_i)$ over several angles of incidence according to Eqs.(8) and (9). We show results for the surface: $D(x) = h[\sin(2\pi x/a) + \cos(6\pi x/a)]$, separating vacuum from a medium of permittivity $\epsilon = 1.5$, $V = -0.5 k_0^2$, $a = 3.18\lambda$, $h = 0.095\lambda$.

Fig. 3 (a) shows the profile $D(x)$, and the integrated intensity $I_T(\mathbf{R}, z_0)$ at four different values of z_0 : $z_0 = [1.25 + 2(n - 1)] h$, $n = 1, 2, 3, 4$ for plane waves incident from the vacuum side. There are 35 incidence angles in the integration; they correspond to incidences of: $-85^\circ, \dots, -10^\circ, -5^\circ, 0^\circ, 5^\circ, 10^\circ, \dots, 85^\circ$. As seen, at near field distances, namely with z_0 close to the surface, at which evanescent components are included in the scattered field wavefront, the integrated intensity $I_T(\mathbf{R}, z_0)$ closely follows the profile $D(x)$; and tends to an almost constant value as these evanescent components are lost by progressively increasing the distance z_0 . By contrast, the resulting $I_T(\mathbf{R}, z_0)$ for just one incident wave (angle of incidence 40°) is shown in Figs 3(b) at the five different values of z_0 given by the above expression with $n = 1, \dots, 5$. We observe once again that as the number of integrated waves increases, the contrast is gradually lost with increasing z_0 . Also, the scattered intensity at low values of z_0 does

not follow the profile, this departure being larger the lower is the number of incidence angles in the integration. In fact, we have observed that the number of lobes in the scattered intensity from one incident wave increases with k and hence does not resemble D .

It should be remarked that, although not shown here for the sake of brevity, calculations on reflection both from penetrable surfaces and hard walls show the same fidelity of surface profile reconstruction by $I_T(\mathbf{R}, z)$. However, we would like to emphasize that in the case of reflection from a hard wall, due to the broader distribution of the angular spectrum as a result of the stronger multiple scattering in this case, the propagating components near the cut-off have a more important role in this case and as a result, as the distance to the surface increases, the integrated intensity tends to a constant more slowly. We have results for several other profiles, but we have chosen to illustrate a generic case with no particular symmetry.

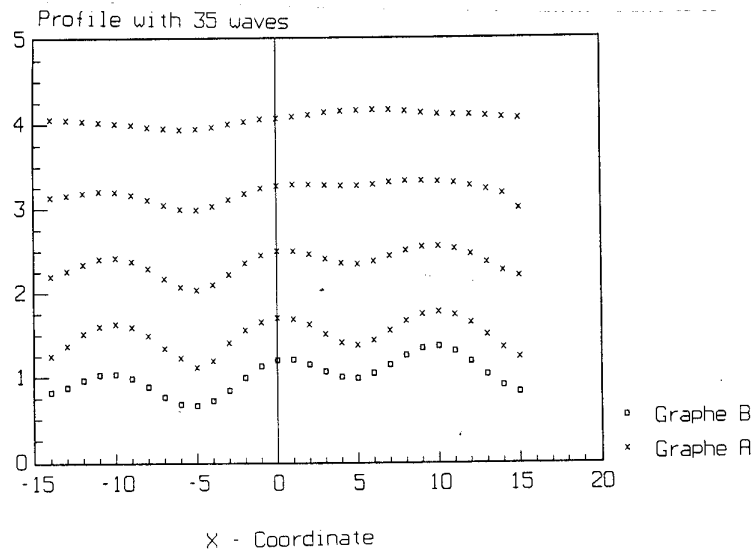


Figure 3(a). Graphe A: Near field scattered intensities averaged over 35 angles of incidence at four distances z_0 given by: $z_0 = [1.25 + 2(n - 1)]h$, $n = 1, 2, 3, 4$. The incident wave impinges from the vacuum side. The permittivity is $\epsilon = 1.5$. Graphe B: Test profile $D(x) = h[\sin(2\pi x/a) + \cos(6\pi x/a)]$, $a = 3.18\lambda$, $h = 0.095\lambda$.

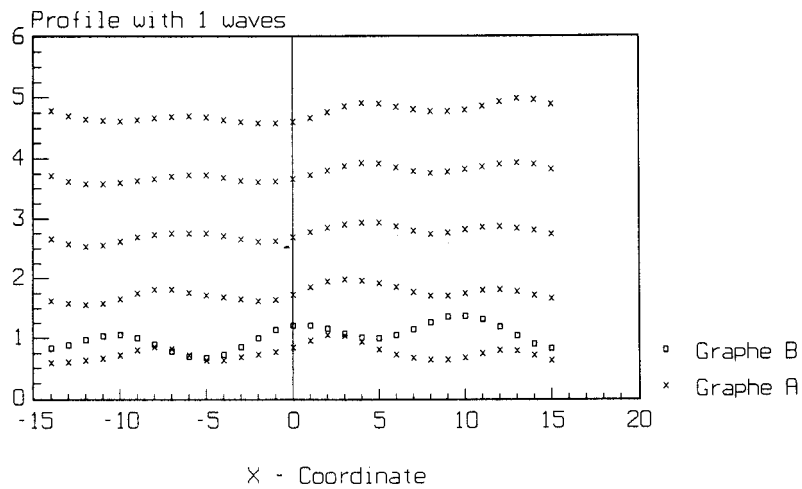


Figure 3(b). Same as Fig. 3(a) for one single incident plane wave at 40° degrees, at five distances with $z_0 = [1.25 + 2(n - 1)]h$, $n = 1, 2, 3, 4, 5$.

4. Conclusion

In conclusion, we have shown that near field scattered intensities integrated over all possible angles of incidence tends to follow the surface profile, more closely the larger is the number and range of integration angles. Thus, while in conventional inverse scattering methods one needs to solve the steps:

$$\text{Scattered intensity} \xrightarrow{P} \text{Scattered amplitude} \xrightarrow{T} \text{Potential}$$

with the transformation P requiring to solve the phase retrieval problem, and the transformation T involving to solve the inverse scattering problem, (T is an inverse Fourier transform only in the case of single scattering, otherwise, one has to devise some skilful method to find T for each specific case), in our procedure, we have:

$$\text{Scattered intensity} \xrightarrow{S} \text{Integrated scattered intensity} \xrightarrow{T=1} \text{Potential}$$

With the operation S being a straightforward integration over all accessible angles of incidence, and the transformation T , which yields the scattering potential, just being unity.

It is worth observing that this integration operation has an averaging effect that destroys the interferences of the multiply scattered waves, and hence amounts to producing an effective incoherent field which is reflected on the surface like in geometrical optics; thus bringing a solution to this inverse scattering problem by means of a kind of classical limit. This constitutes a dramatic simplification to the problem of determining the profile of a surface from scattering data, since, on the one hand, it does not require to perform phase retrieval, neither to devise an inverse scattering method to invert the scattered field data.

Acknowledgments

This research has been supported by grants from the CICYT through grants PB 92-0081 and MAT 92.0129 the EC grant SCI 0395 C.

References

- [1] D. Gabor, Proc. Roy. Soc. Lond. A **197**, 454 (1949).
- [2] J.W. Goodman, *Introduction to Fourier Optics* (Mac Graw Hill, New York, 1968).
J.C. Dainty and R. Shaw, *Image Science* (Academic Press, New York, 1974).
- [3] A. Tonomura, Rev. Mod. Phys. **59**, 639 (1987); F.G. Missiroli, G. Pozzi, and U. Valdre, J. Phys. E: Sci. Instrum. **14**, 649 (1981).
- [4] E. Wolf, Opt. Comm. **1**, 153 (1969); R.P. Porter, in *Progress in Optics*, edited by E. Wolf (North-Holland, Amsterdam, 1989).
- [5] M. Nieto-Vesperinas, *Scattering and Diffraction in Physical Optics*, (J. Wiley, New York, 1991).
- [6] R.P. Millane, J. Opt. Soc. Am. **7**, 394 (1990).

- [7] J.R. Fienup, in *International Trends in Optics*, edited by J.W. Goodman, (Academic Press, New York, 1991).
- [8] H. P. Baltes, ed., *Inverse Scattering Problems in Optics*, Topics in Current Physics, Vol. 9, Springer-Verlag, Berlin, 1978.
- [9] K. Chadan and P.C. Sabatier, *Inverse Problems in Quantum Scattering Theory*, Springer-Verlag, Berlin, 1989, 2nd Edition.
- [10] W.M. Boerner, ed., *Inverse Methods in Electromagnetic Imaging*, N.A.T.O. A.S.I. Series, Serie C, Vol. 143, Reidel, Dordrecht, 1985.
- [11] A. Howie, *Nature* **345**, 386 (1990).
- [12] P. Hu and D.A. King, *Nature* **360**, 655 (1992).
- [13] N. Garcia and M. Nieto-Vesperinas, *Opt. Lett.* **18**, 2090 (1993).
- [14] N. Garcia and M. Nieto-Vesperinas, *Phys. Rev. Lett.* **71**, 3645 (1993).
- [15] N. Garcia and N. Cabrera, *Phys. Rev. B* **18**, 576 (1978).
- [16] E. Wolf, *Opt. Comm.* **1**, 153 (1969); R.P. Porter, in *Progress in Optics*, E. Wolf, ed., North-Holland, Amsterdam, 1989.
- [17] D. Marcuse, *Light Transmission Optics*, 2nd ed., Van Nostrand Reinhold, New York, 1982.
- [18] J.M. Bennett and L. Mattsson, *Introduction to Surface Roughness and Scattering*, Optical Society of America, Washington D.C., 1989; J.M. Bennett, ed., *Surface Finish and its Measurement* Optical Society of America, Washington D.C., 1992; J.C. Dainty, in *Modern Trends in Optics*, J.W. Goodman, editor, Academic Press, New York, 1991.
- [19] J.A. de Santo and G.S. Brown, in *Progress in Optics* vol.23, E. Wolf, ed., (North-Holland, Amsterdam, 1986), pp.2-62; M. Nieto-Vesperinas and J.C. Dainty, eds., *Scattering in Volumes and Surfaces*, (North-Holland, Amsterdam, 1990); J.A. Ogilvy, *Theory of Wave Scattering from Random Rough Surfaces* (Adam Hilger, Bristol, 1991); R.J. Wombell and J.A. de Santo, *J. Opt. Soc. Am. A* **8**, 1892 (1991).
- [20] L. Tsang, J.A. Kong and R.T. Shin, *Theory of Microwave Remote Sensing*, J. Wiley, New York, 1985.
- [21] B.V. Grinyov and V.L. Yankelevich, *Nucl. Instr. Meth. A* **306**, 229 (1991).
- [22] D. W. Pohl, W. Denk and M. Lanz, *Appl. Phys. Lett.* **44**, 651 (1984); D. W. Pohl, **Advances in Optical and Electron Microscopy**, C. J. R. Sheppard and T. Mulvey, eds. (Academic Press, New York, 1990), pp. 243-312.
- [23] G. A. Massey, *Appl. Opt.* **23**, 658 (1984).
- [24] E. Betzig, A. Harootunian, A. Lewis and M. Isaacson, *Appl. Opt.* **25**, 1890 (1986); E. Betzig, J. K. Trautman, J. S. Weiner, T. D. Harris and R. Wolfe, *Appl. Opt.* **31**, 4563 (1992); E. Betzig, and J. K. Trautman, *Science* **257**, 189 (1992).

- [25] J. M. Vigoureux, C. Girard and D. Courjon, *Opt. Lett.* **14**, 1039-1041 (1989); D. Courjon, K. Sarayeddine and M. Spajer, *Opt. Comm.* **71**, 23 (1989).
- [26] E. Wolf and M. Nieto-Vesperinas, *J. Opt. Soc. Am A* **2**, 886 (1985).
- [27] R. F. Millar, *Proc. Camb. Phil. Soc.* **65**, 773 (1969).
- [28] M. Nieto-Vesperinas and N. Garcia, *Opt. Acta* **28**, 1651 (1991).
- [29] K.H. Rieder, N. Garcia and V. Celli, *Surf. Sci.* **108**, 169 (1981).